Therapeutics, Targets, and Chemical Biology

Cancer Research

A Therapeutic Anti–VEGF Antibody with Increased Potency Independent of Pharmacokinetic Half-life

Yik Andy Yeung[1], Xiumin Wu[2], Arthur E. Reyes II[3], Jean-Michel Vernes[4], Samantha Lien[1], John Lowe[5], Mauricio Maia[5], William F. Forrest[6], Y. Gloria Meng[4], Lisa A. Damico[3], Napoleone Ferrara[2], and Henry B. Lowman[1]

Abstract

Bevacizumab [Avastin; anti–vascular endothelial growth factor (VEGF) antibody] is an antiangiogenic IgG approved for treating patients with certain types of colon, breast, and lung cancer. In these indications, bevacizumab is administered every 2 to 3 weeks, prompting us to study ways to reduce the frequency of administration. Increasing affinity to neonatal Fc receptor (FcRn) may extend the pharmacokinetic half-life of an antibody, but the quantitative effect of FcRn affinity on clearance has not been clearly elucidated. To gain further insight into this relationship, we engineered a series of anti-VEGF antibody variants with minimal amino acid substitutions and showed a range of half-life improvements in primates. These results suggest that, if proven clinically safe and effective, a modified version of bevacizumab could potentially provide clinical benefit to patients on long-term anti-VEGF therapy through less-frequent dosing and improved compliance with drug therapy. Moreover, despite having half-life similar to that of wild-type in mice due to the species-specific FcRn binding effects, the variant T307Q/N434A exhibited superior *in vivo* potency in slowing the growth of certain human tumor lines in mouse xenograft models. These results further suggest that FcRn variants may achieve increased potency through unidentified mechanisms in addition to increased systemic exposure. *Cancer Res; 70(8); 3269–77. ©2010 AACR.*

Introduction

The development and use of therapeutic antibodies to treat cancer has increased dramatically in recent years, including, for example, bevacizumab [Avastin; anti–vascular endothelial growth factor (VEGF) antibody] as an antiangiogenic agent in the treatment of several types of malignancies (1). In addition to offering highly specific, high-affinity binding interactions with their antigens, IgGs have an advantage over other biologics and small molecules in that they persist in the circulation with long systemic half-lives, mediated by the pH-dependent interaction with the neonatal Fc receptor (FcRn; refs. 2–7). Multiple genetic knockout and knock-in experiments in mice have confirmed that FcRn is important for the homeostasis and transcytosis of IgGs (8–13).

Authors' Affiliations: Departments of [1]Antibody Engineering, [2]Tumor Biology and Angiogenesis, [3]Early Development Pharmacokinetics and Pharmacodynamics, [4]Assay and Automation Technology, [5]BioAnalytical Research and Development, and [6]Biostatistics, Genentech, Inc., South San Francisco, California

Note: Supplementary data for this article are available at Cancer Research Online (http://cancerres.aacrjournals.org/).

Corresponding Author: Henry B. Lowman, NGM Biopharmaceuticals, 630 Gateway Boulevard, South San Francisco, CA 94080. Phone: 650-243-5577; Fax: 650-583-1646; E-mail: hlowman@ngmbio.com.

doi: 10.1158/0008-5472.CAN-09-4580

Therapeutic antibodies with extended half-life offer the potential benefit of lower frequency of administration. Modulating the interaction between Fc and FcRn through protein engineering may improve the pharmacokinetics of antibodies (14–22) through increased pH 6 affinity. However, increased pH 7.4 affinity may hinder the release of IgG variants and offset any pharmacokinetic improvement (14, 22). Hitherto, the detailed relationship between FcRn affinity and half-life has not been elucidated, as previous studies have focused on a small number of variants, within a limited range of FcRn affinities. Therefore, the maximal IgG1 half-life extension achievable through engineering the Fc-FcRn interaction has been unclear. Previously, in primate studies of a different antibody (targeting a cell surface receptor), we found that a human IgG1 Fc variant (N434A) with 3-fold increased FcRn binding at pH 6.0 had modestly improved pharmacokinetics over wild-type (WT); however, another Fc variant (N434W), which had ~40-fold affinity improvement, did not exhibit improved pharmacokinetics (22). We were therefore motivated to study additional antibody variants with intermediate binding affinities for primate FcRn.

Here, we constructed five Fc variants with varying FcRn affinities on bevacizumab (1, 23), a humanized anti-VEGF–A (or VEGF) IgG1 antibody, to perform a comprehensive pharmacokinetic study in cynomolgus monkeys using large cohorts (n = 12 animals per group) to detect modest pharmacokinetic changes, as well as comparative efficacy studies in mice expressing a humanized form of VEGF-A. Our results

identify the optimal range of FcRn affinity for an Fc variant to achieve maximal half-life extension in primates, with the serum half-life of our most-improved Fc variant, T307Q/N434A, measuring ~25 days under the conditions of this study in cynomolgus monkeys.

We also compared the *in vivo* tumor inhibition activities of the WT bevacizumab antibody and the T307Q/N434A variant in mouse xenograft studies. Paradoxically, despite having no systemic half-life improvement in mice due to the species-specific nature of FcRn binding, the T307Q/N434A variant exhibited superior potency in treating selected human tumor xenografts in mice. Our work suggests more generally that an antibody Fc variant engineered for improved FcRn affinity may achieve improved potency via new mechanism(s) in addition to increased persistence in serum.

Materials and Methods

Expression of anti-VEGF antibodies and FcRn. Selected Fc mutations were incorporated into anti-VEGF IgG1 using Kunkel-based mutagenesis as previously described (24). Briefly, heavy and light chain cDNAs encoding each antibody were transiently transfected into Chinese hamster ovary (CHO) cells, and the antibodies were purified over protein A columns followed by size exclusion chromatography. Extracellular domains of human, cynomolgus monkey, and murine FcRn were expressed in 293 or CHO cells as previously described (22).

FcRn binding studies using surface plasmon resonance. The binding affinities of the antibodies to human and cynomolgus monkey FcRn were determined using a BIAcore 3000 instrument (GE Healthcare) as previously described (22). Briefly, the antibodies were conjugated directly onto the CM5 sensor chips using an amine coupling kit, and FcRn was injected over the antibody-conjugated flow cell. The kinetic parameters and dissociation constants (K_D) were then determined using the BIAevaluation software.

Pharmacokinetics in cynomolgus monkeys. Naive cynomolgus monkeys, weighing 2 to 5 kg and 2 to 7 y in age, were assigned to six treatment groups, each consisting of six males and six females. All animals received on day 1 a single i.v. bolus dose of 5 mg/kg via the saphenous vein followed by a 0.9% saline flush. Blood samples (~1.0 mL) from the femoral vein were collected before and after dose at 0.5, 2, 4, and 8 h and at 1, 2, 4, 7, 10, 14, 21, 28, 35, 42, 49, 56, and 70 d. The study was conducted at Covance under standard operating procedures and in compliance with applicable regulations about the use of laboratory animals.

Serum antibody concentrations were detected using a VEGF capture ELISA (25, 26). Briefly, Maxisorp ELISA plates (Thermo Fisher Scientific) were coated with 0.5 μg/mL of recombinant human VEGF. Two-fold serially diluted standards (0.20–25 ng/mL) as well as 3-fold serially diluted cynomolgus monkey serum samples (minimum 1:10 dilution) were added to the blocked plates and incubated for 2 h at room temperature with shaking. Bound drug was detected by incubation with sheep anti-human IgG–horseradish peroxidase (HRP; diluted 1:2,000; The Binding Site) for 1 h at room temperature. The plates were then developed with tetramethylbenzidine substrate (Moss). The plates were read on a microplate reader at a wavelength of 450 to 620 nm.

Pharmacokinetic parameters for cynomolgus monkeys were estimated using WinNonlin Enterprise version 5.1.1 (Pharsight Corp.). A two-compartment model with i.v. bolus input, first-order elimination, and microrate constants (Model 7) was used to describe the observed data for individual cynomolgus monkey concentration-time profiles. Concentrations were weighted using iterative reweighting (1/y) and the Gauss-Newton minimization algorithm with Levenberg and Hartley modification. Differences in mean $t_{1/2,\beta}$ were analyzed using the Tukey-Kramer honestly significant difference correction for multiple comparisons, executed via the multcomp v 1.0-2 package in R version 2.7.2 (R Development Core Team, 2008).

Pharmacokinetics in VEGF knock-in mice. Rag2 KO; hum-X VEGF KI mice (27) were assigned to four groups with eight to nine animals per group; a 0.3 mg/kg and a 5 mg/kg dose group were designated for the bevacizumab WT and T307Q/N434A variant. Each animal received a single i.v. dose of either 0.3 or 5 mg/kg of antibody via the tail vein. Blood samples from three mice were collected at 15 min; at 8 and 24 h; and at 2, 4, 7, 10, 14, 21, and 28 d after dose. Serum antibody concentrations were detected similarly as described for cynomolgus monkey serum samples using a VEGF capture ELISA, except goat anti-human Fc HRP (Jackson) was used for detection. Group mean serum antibody concentration-time profiles were used to estimate pharmacokinetic parameters in mice using WinNonlin Enterprise, version 5.1.1. To estimate pharmacokinetic parameters, a two-compartment elimination model with i.v. bolus input and first-order elimination, and with microrate constants, was used to describe the observed data (WinNonlin Model 7). Concentrations were weighted using iterative reweighting (1/y) and the Nelder-Mead minimization algorithm. A naive pooled approach was used with all observed data to provide one estimate for each treatment group. All procedures used in the mouse pharmacokinetic and mouse efficacy studies followed protocols approved by the Institutional Animal Care and Use Committee.

In vivo *efficacy studies.* Growth conditions of HM-7 (colorectal carcinoma) and Calu-6 (lung carcinoma) cells were previously described (28). Human HT-55 (colorectal carcinoma) was grown in RPMI 1640 supplemented with 10% (v/v) fetal bovine serum, 1% (v/v) penicillin/streptomycin (Invitrogen), 2 mmol/L L-glutamine (Invitrogen), and 1 μg/mL fungizone (Invitrogen). Cells were grown at 37°C in 5% CO_2 until confluent, harvested, and resuspended in sterile Matrigel at 50×10^6/mL. Xenografts were established in 6- to 8-wk-old Rag2 KO; hum-X VEGF KI double-homozygous mice (Genentech; ref. 27) by dorsal flank s.c. injection of 5×10^6 cells per mouse and allowed to grow. Antibodies were administered i.p. at the dose of 5, 0.5, and 0.05 mg/kg twice weekly 24 h after tumor cell inoculation. The transplanted tumors were measured twice weekly as described (28). Tumor volume for each mouse was calculated after each measurement, and the mean tumor volumes from different treatment groups were compared by Student's *t* test, with significance

identified at a level of $P < 0.05$. Blood samples were also collected for pharmacokinetic analysis. Mice were sacrificed when tumor volume reached 2,000 mm^3. At the end of treatment, tumors were excised, weighed, and then homogenized. The total protein contents in tumor homogenates were determined using Bradford Coomassie assay (Pierce) according to the manufacturer's protocol. Antibody concentrations in the serum and tumor homogenates were measured in an ELISA using rabbit anti-Fc capture (Jackson) and goat anti-human Fc-HRP (Jackson) for detection.

FcRn immunoprecipitation using a high-affinity IgG1 variant. Five million cells per each of either HM-7, HT-55, Calu-6, or Raji (B-cell lymphoma) lines were lysed by incubating in 25 mmol/L sodium phosphate buffer (pH 6.0) containing 1% NP40, 0.5% sodium deoxycholate, 0.1% SDS, 2 mmol/L EDTA, 150 mmol/L NaCl, and 1× protease inhibitor (Pierce) for 1 h at 4°C. Lysed cells were centrifuged and then 50 nmol/L trastuzumab Fc variant M252Y/V308P/N434A (22) was added to the supernatant to capture the FcRn at 4°C. Protein-L (Pierce) resin was then added and washed. Bound proteins were eluted with a 2× loading buffer (Invitrogen) and detected in Western blot using 1 ng/mL of rabbit anti- human FcRn antibody (Santa Cruz Biotechnology) and goat anti-rabbit IgG-peroxidase conjugate at $1:10^4$ dilution (Pierce).

Results

Design, construction, and* in vitro *characterization of anti-VEGF Fc variants. To probe how FcRn affinity affects half-life, five anti-VEGF antibody variants with K_D (equilibrium dissociation constant; see Materials and Methods) improvements of 5- to 35-fold for primate FcRn binding were designed using combinations of mutations at four Fc sites: N434H, T307Q/N434A, T307Q/N434S, T307Q/E380A/N434S, and V308P/N434A [Fc positions are indicated by EU numbering; WT residues (preceding the position) and mutations (following) are shown in single-letter code].

The binding affinities of the anti-VEGF antibodies to primate FcRn were first determined using surface plasmon resonance. The K_D of the WT IgG for cynomolgus monkey and human FcRn (Table 1 and Supplementary Table S1, respectively) agreed well with previous values for other human IgG1s (14, 16). The IgG variants exhibited about 5- to 35-fold and 4- to 26-fold increases in pH 6.0 affinity over WT to cynomolgus monkey FcRn and to human FcRn, respectively. Three variants previously studied in the context of trastuzumab (Herceptin; anti-HER2 monoclonal antibody)—namely, N434H, T307Q/N434A, and V308P/N434A—also corresponded well with previous measurements versus trastuzumab (22). The pH 7.4 affinity ranking of all these antibodies was the same as that at pH 6.0 (Supplementary Fig. S1), indicating similar pH dependency of FcRn binding and release. Overall, the affinity increase for each variant was comparable for cynomolgus monkey and human FcRn.

Table 1 shows that the increase in FcRn affinity among the variants was largely due to a decrease in k_{off}, and the pH dependence of k_{off} was similar for each variant (Supplementary Fig. S2). All of the variants were confirmed to have the same VEGF binding affinity. They also inhibited VEGF-induced *in vitro* human umbilical vascular endothelial cell proliferation as effectively as bevacizumab (Supplementary Fig. S3), consistent with the fact that they contain identical variable domains for binding VEGF.

Pharmacokinetics of anti-VEGF Fc variant antibodies in cynomolgus monkeys. The pharmacokinetics of anti-VEGF WT and five variants were examined in cynomolgus monkeys (n = 12 animals per group) following a single i.v. dose of 5 mg/kg. The average serum concentration-time profiles and tabulated half-lives are shown in Fig. 1A and Table 1, respectively. The WT bevacizumab studied here had a terminal half-life ($t_{1/2,\beta}$) of 11.4 ± 1.5 days and a clearance rate (CL) of 4.01 ± 0.67 mL/d/kg (Supplementary Table S2), both of which are comparable with the previously obtained data for Avastin in cynomolgus monkeys (29). All of the variants exhibit

Table 1. The binding parameters (monovalent IgG–FcRn) of the anti–VEGF-A human IgG1 WT and variants against cynomolgus monkey FcRn and their respective half-lives in cynomolgus monkey

Fc variant	k_{on} (×10^5 mol/L^{-1} s^{-1})	k_{off} (×10^{-2} s^{-1})	K_D (nmol/L)*	K_D (nmol/L)†	Half-life (d)
WT	2.7 ± 0.9	63 ± 21	2,400 ± 100	2,400 ± 100	11.4 ± 1.5
N434H	4.8 ± 0.7	21.8 ± 3.3	450 ± 10	470 ± 10	18.6 ± 4.9‡
T307Q/N434A	4.7 ± 0.1	11.2 ± 0.4	240 ± 9	241 ± 5	24.9 ± 4.7‡
T307Q/N434S	4.4 ± 0.2	8.5 ± 0.1	195 ± 5	203 ± 6	22.4 ± 3.9‡
T307Q/E380A/N434A	4.3 ± 0.1	6.6 ± 0.3	153 ± 4	160 ± 4	21.7 ± 4.5‡
V308P/N434A	5.1 ± 0.2	3.4 ± 1.2	66.6 ± 1.8	69.9 ± 2.3	20.5 ± 5.0‡

NOTE: FcRn binding was performed at pH 6.0 and 25°C using BIAcore. Results are shown as mean ± SD (n = 3). Half-life parameters were tabulated from the serum concentration-time curves shown in Fig. 1A. Results are shown as mean ± SD (n = 11 or 12).

*Determined by ratio of k_{off} to k_{on}.

†Determined by fitting the steady-state response against concentration.

‡Statistically significant from the half-life of WT ($P < 0.001$).

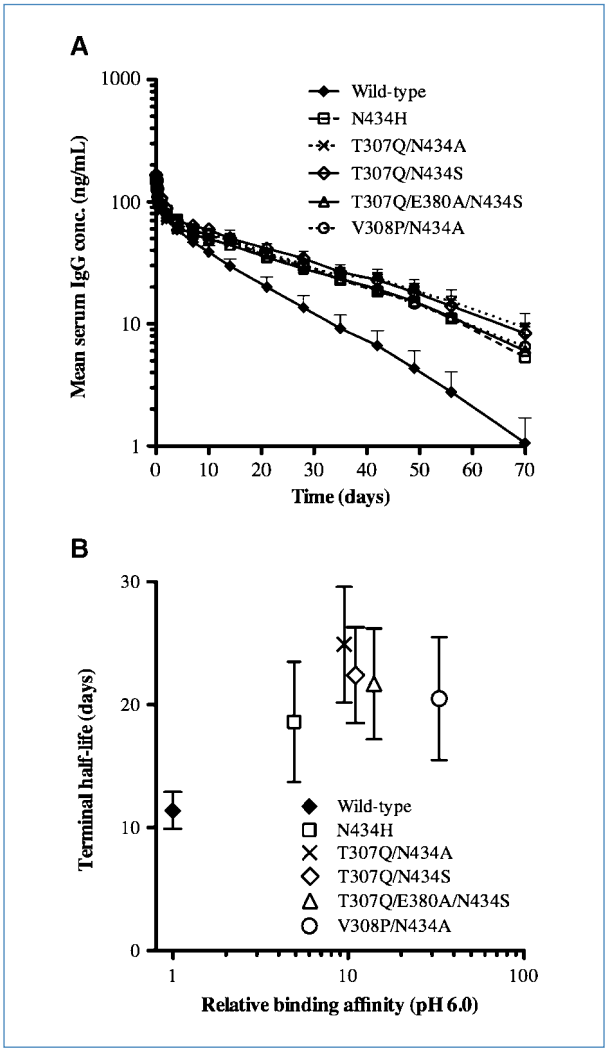

Figure 1. Pharmacokinetics of the anti–VEGF-A WT and five Fc variants in cynomolgus monkeys. A, serum concentrations of the antibodies were measured by ELISA following a single i.v. injection of 5 mg/kg. Points, mean (n = 12 animals per group, except for the V308P/N434A group, which had 11 animals); bars, SD. B, relationship between human IgG1 terminal half-life in cynomolgus monkeys and pH 6.0 FcRn affinity. Relative K_D values (ratio of variant to WT) and half-life data are from Table 1. The difference in half-life of each variant compared with WT is statistically significant, as is the difference in half-life of N434H and T307Q/N434A (see text for details).

increased drug exposure (area under the curve), increased $t_{1/2,\beta}$, and reduced CL compared with WT ($P < 0.001$), with T307Q/N434A having the greatest improvement in $t_{1/2,\beta}$ (Table 1; Supplementary Table S2).

The relationship between terminal half-life in cynomolgus monkey and pH 6.0 K_D is depicted in Fig. 1B. These results agree with previous observations that modest increases in pH 6.0 affinity yield prolonged $t_{1/2,\beta}$ (15, 16, 18), as evidenced by N434H and T307Q/N434A. Intriguingly, Fig. 1B shows that additional increases in pH 6.0 affinity beyond 10-fold (i.e., in the case of T307Q/N434S, T307Q/E380A/N434A, and V308P/N434A) do not offer further improvement in half-life; instead, there is an insignificant trend toward reduced half-life at higher affinities. Our results therefore suggest that ~10-fold increased relative affinity for primate FcRn, as measured here for T307Q/N434A, may offer maximal half-life improvement in primates.

Pharmacokinetics of anti-VEGF WT and T307Q/N434A in mice. Because murine and primate FcRn have different affinities for human IgG1 as well as for Fc variants, a pharmacokinetic study in nontumor-bearing, genetically engineered mice (expressing a humanized form of VEGF-A; see below) was performed as a prelude to mouse efficacy studies. As shown in Fig. 2, despite having higher murine FcRn affinity at both pH 6.0 and pH 7.4 (Supplementary Table S3; Supplementary Fig. S4), the selected variant T307Q/N434A exhibits similar clearance and half-life as WT in mice (Supplementary Table S4) using two different dosage groups. These results imply that any potential difference in pharmacodynamics between WT and T307Q/N434A does not result from systemic clearance differences.

In vivo *potency of anti-VEGF WT and T307Q/N434A in mice.* Having established similar pharmacokinetics for these two antibodies in mice, we compared their *in vivo* potency and efficacy in treating human tumor xenografts grown in immunocompromised knock-in mice expressing a humanized form of VEGF-A (Rag2 KO; hum-X VEGF KI mice; ref. 27). Such mice are useful for making comparisons with bevacizumab because this antibody does not recognize murine VEGF, which is often a stromal component of tumor growth. WT and T307Q/N434A antibodies were tested in inhibiting the growth of HM-7 (colorectal carcinoma), HT-55 (colorectal carcinoma), and Calu-6 (lung carcinoma) human tumor xenografts in Rag2 KO; hum-X VEGF KI mice. Figure 3A shows that, at a dose of 5 mg/kg, T307Q/N434A is equally efficacious as WT in inhibiting the growth of HM-7 tumors.

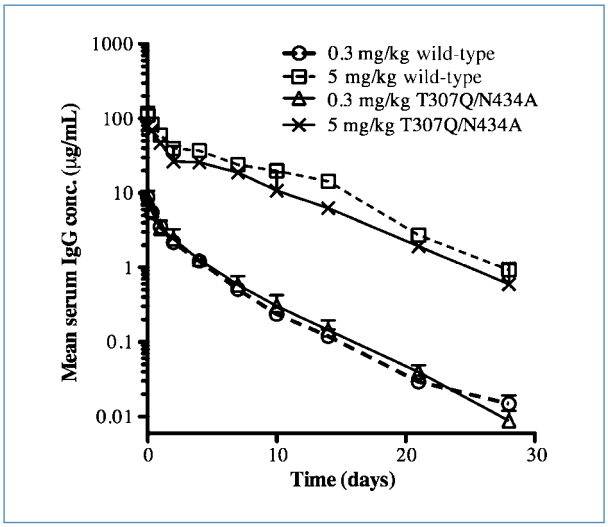

Figure 2. Pharmacokinetics of the anti–VEGF-A WT and T307Q/N434A in Rag2 KO; hum-X VEGF KI mice. Serum concentrations of the antibodies were measured by ELISA following a single i.v. dose of 5 or 0.3 mg/kg. Points, mean of three animals; bars, SD.

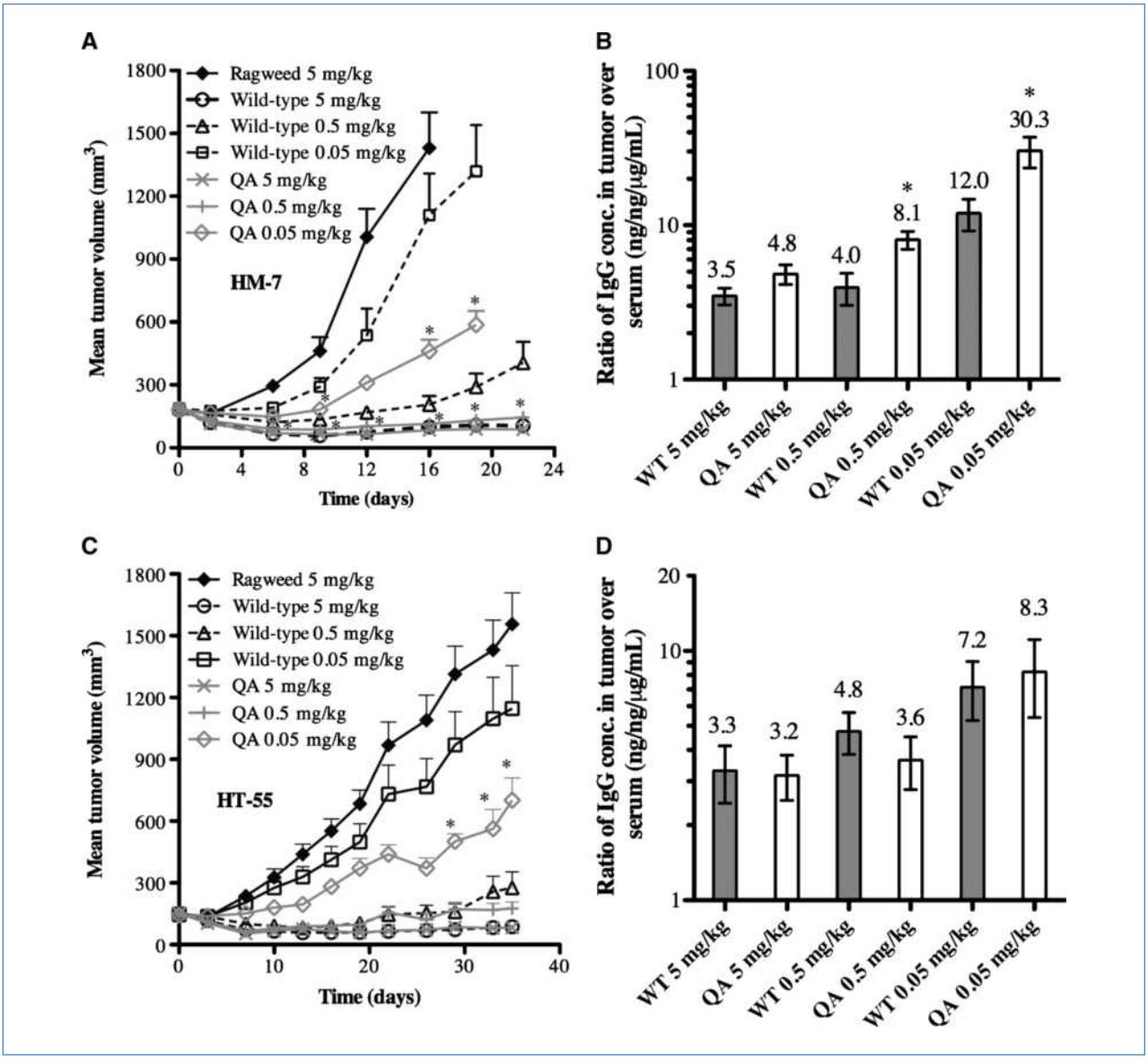

Figure 3. Efficacy of anti–VEGF-A WT and T307Q/N434A variant antibodies in treating human colorectal tumor xenografts implanted in Rag2 KO; hum-X VEGF KI mice. Doses of 5, 0.5, and 0.05 mg/kg of WT or T307Q/N434A (QA), or 5 mg/kg of anti-ragweed control, were administered i.p. twice weekly. Colorectal tumor lines were HM-7 (A and B) or HT-55 (C and D). *, $P < 0.05$, statistically significant differences between WT and variant by dose. A, growth curves of HM-7 tumors. Points, mean tumor volumes ($n = 10$); bars, SE. B, ratio of antibody concentration in HM-7 tumors to that in serum at the end of treatment. Antibody concentration in the tumor represented the amount of anti–VEGF-A antibody in tumor lysates normalized by the total protein. Columns, mean ($n = 10$); bars, SE. C, growth curves of HT-55 tumors. Points, mean tumor volumes ($n = 10$); bars, SE. D, ratio of antibody concentration in tumors to that in serum for HT-55. Columns, mean ($n = 5$); bars, SE. For 5 mg/kg treatment groups, both anti–VEGF-A WT and T307Q/N434A treatments are significantly different ($P < 0.001$) from the anti-ragweed treatment in both xenograft models.

Surprisingly, similar inhibition of HM-7 tumor growth was observed at the 0.5 mg/kg dose of T307Q/N434A as at the 5 mg/kg dose of WT. This increase in potency (i.e., equal effect at lower dose) was not due to differences in serum antibody concentrations between WT and T307Q/N434A, as concentrations of both antibodies in multiple serum samples taken during the treatment were comparable (data not shown), consistent with the mouse pharmacokinetic data described above. However, we did observe statistically significant increases in the antibody concentrations within the tumors for the 0.5 and 0.05 mg/kg T307Q/N434A-treated groups compared with the corresponding WT groups (Fig. 3B). The HM-7 xenograft study was repeated two more times, and increased potency for the variant over WT was similarly observed in both additional studies (Supplementary Figs. S5 and S6).

Both antibodies also achieved complete inhibition of the HT-55 and Calu-6 tumor growth at 5 mg/kg. For the HT-55

xenografts (Fig. 3C and D), we noted a less significant trend toward improved potency than with HM-7, whereas for the Calu-6 xenografts (Fig. 4A and B), there was no observed difference in potency. This lack of significantly improved potency for HT-55 and Calu-6 relative to HM-7 was perhaps due to an absence of preferential accumulation of the variant within the tumor (Fig. 3D). We subsequently found that all three cell lines examined in this study showed considerably high level of FcRn expression (Fig. 4C; also supported by our in-house microarray data; data not shown). However, the increased concentration of variant detected in the HM-7 tumors relative to the HT-55 and Calu-6 tumors is not directly correlated with cellular FcRn expression level, as HM-7 cells express lower amounts of FcRn than either HT-55 or Calu-6 cells (Fig. 4C); indeed, Western blots showed that the FcRn expression levels in HT-55 and Calu-6 are about 50% and 10% higher than that in HM-7, respectively.

Discussion

In this work, we engineered five anti-VEGF antibody variants with K_D improvements for primate FcRn ranging from 5- to 35-fold compared with bevacizumab. By determining the half-lives of these variants *in vivo*, we established a quantitative picture of how FcRn affinity affects IgG1 half-life in cynomolgus monkeys (Fig. 1B). Our results show that a moderate increase in pH 6.0 affinity, up to 10-fold, yields extended half-life, and suggest that further affinity increases will not further increase half-life. Rapid clearance has been observed in mouse pharmacokinetic studies using some high-affinity human IgG1 variants (14, 19) and also recently shown in a cynomolgus monkey pharmacokinetic study of a 40-fold increased affinity variant (22). The diminishing half-life returns of increased FcRn affinity at pH 6.0 among these variants are most likely due to their corresponding increases in neutral pH binding (Supplementary Figs. S1 and S2), preventing the efficient release of FcRn-bound IgG back into circulation and increasing the internalization of serum IgG into the cells (5–7, 30, 31), and effectively offsetting the pharmacokinetic advantage gained by binding increases at pH 6.0.

The half-life of T307Q/N434A, having ~10-fold increased FcRn affinity at pH 6.0 compared with bevacizumab, was ~25 days in our primate study, corresponding to a 2.2-fold half-life extension. In comparison, a previously reported M252Y/S254T/T256E variant of humanized anti–respiratory syncytial virus (RSV; ref. 16), which showed 9-fold increase in pH 6.0 FcRn affinity, had slightly shorter half-life (21 days; a reported 3.5-fold extension) than that of the T307Q/N434A anti-VEGF antibody in our study. This apparent inconsistency may be due to the 2-fold shorter half-life of the WT anti-RSV compared with WT anti-VEGF (bevacizumab), possibly arising from a variety of factors (see below). Our results argue that an Fc variant should have a pH 6.0 K_D of ~240 nmol/L as measured in the binding assay described here to achieve maximal half-life extension in primates.

Along with FcRn affinity, other factors, such as antibody stability and specific clearance mechanisms (e.g., antigen-dependent clearance), can influence the pharmacokinetics

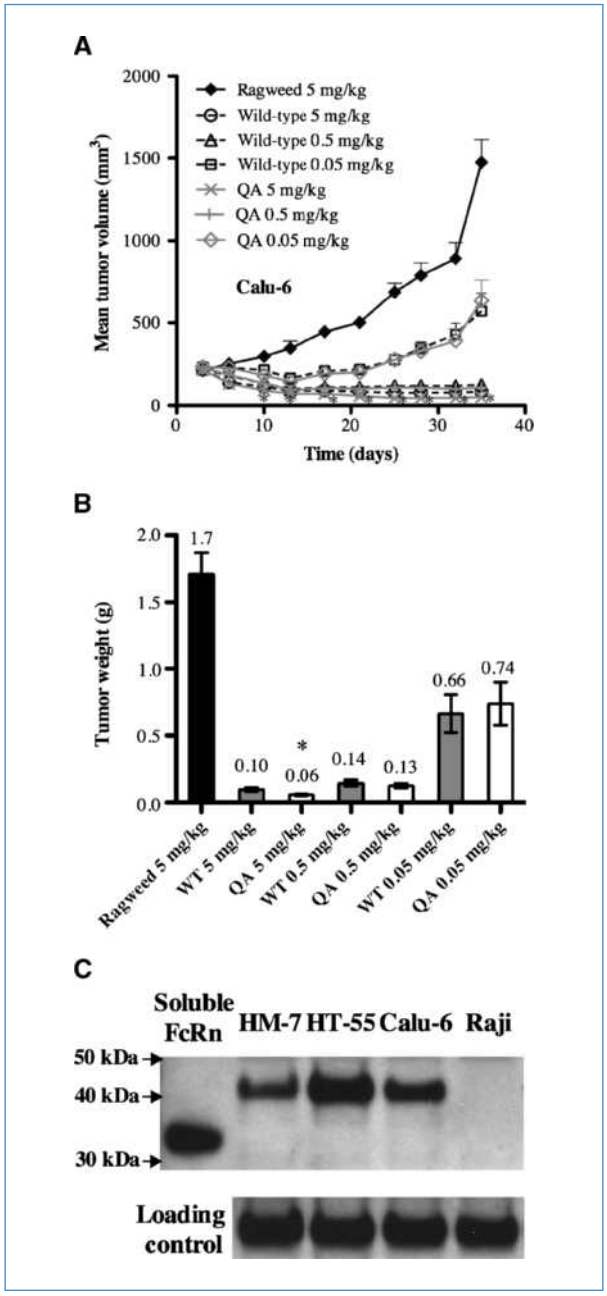

Figure 4. Efficacy of anti–VEGF-A WT and T307Q/N434A variant antibodies in treating human Calu-6 (lung) xenografts implanted in Rag2 KO; hum-X VEGF KI mice. Doses of 5, 0.5, and 0.05 mg/kg of WT or T307Q/N434A, or 5 mg/kg of anti-ragweed control, were administered i.p. twice weekly. A, growth curves of Calu-6 tumors. Points, mean (n = 10); bars, SE. B, terminal weights of Calu-6 tumors determined at the end of treatment (day 35). Columns, mean (n = 10); bars, SE. For 5 mg/kg treatment groups, both anti–VEGF-A WT and T307Q/N434A treatments are significantly different ($P < 0.001$) from the anti-ragweed treatment group. C, expression levels of FcRn in different human tumor cell lines. Raji cells (human B-cell lymphoma) were used as a negative control, whereas soluble human FcRn protein, which is missing the 7-kDa transmembrane and cytoplasmic regions, was blotted as a positive control. Dilutions of soluble FcRn protein were used as the standard to quantify the FcRn expression level. Results shown here are representative of at least three independent experiments.

of human(ized) IgGs (20, 32, 33), and animal-to-animal variability complicates pharmacokinetic comparisons (note: n = 12 animals per group in our primate pharmacokinetic study). However, we contend that the optimal FcRn affinity should be generalizable to IgGs in which nonspecific mechanisms constitute the major mechanism of antibody clearance. We predict that the affinity-versus-pharmacokinetics relationship in cynomolgus monkey will apply to humans, and several observations support this: human and cynomolgus monkey FcRn share >95% sequence identity, they bind human IgG1 with similar affinity and pH dependence, and they bind all of the anti-VEGF variants studied here with similar affinity.

In contrast to our primate pharmacokinetic results, in our mouse pharmacokinetic studies, due to species-specific binding of murine FcRn (34), the anti-VEGF variant T307Q/N434A showed similar clearance as WT, and hence, we expected the variant to have similar potency in mice xenograft studies. Indeed, similar potency was observed in the Calu-6 tumor model (Fig. 4).

However, most surprisingly, in our further mouse efficacy studies, T307Q/N434A exhibited superior potency in treating selected tumor lines, namely, in three iterations of the HM-7 tumor model (Fig. 3A and B; Supplementary Figs. S5 and S6) as well as in the HT-55 tumor model (Fig. 3C and D) at 0.05mg/kg. This potency increase was not due to a difference in FcγR binding affinity or complement activity between WT and T307Q/N434A, nor any detectable nonspecific binding of either antibody to HM-7 cells at either pH 6.0 or 7.4 (data not shown). Instead, the potency increase correlated with increased concentration of antibody variant within certain tumors compared with WT antibody (Fig. 3B and D). This potency increase was apparently not a result of elevated clearance in the WT groups, as antibody concentrations in serum samples taken from both WT and variant-treated mice at various time points during the experiment were similar to those estimated by using the pharmacokinetic parameters from nontumor-bearing mice (data not shown). Terminal serum concentrations were also similar in animals treated with WT or variant (see Supplementary Figs. S5B and S6C).

We hypothesize that the increased potency of the variant in certain mouse xenografts (e.g., HM-7) could be due to increased retention and/or recycling of the variant antibody mediated in part by the human FcRn expressed in these tumors. This may simply lead to an increased mass action effect of blocking locally produced VEGF or may provide a mechanism for enhanced degradation of VEGF in the tumor. Previously, another Fc variant with improved human FcRn binding was shown to have slower degradation rate and improved recycling behavior than WT *in vitro*, in human tumor cells expressing FcRn (35). In a perhaps related finding, Dall'Acqua and colleagues (16) reported that the concentration of the anti-RSV variant M252Y/S254T/T256E in the bronchoalveolar lavage of cynomolgus monkeys increased proportionally with the rise of serum IgG level. This tissue-specific accumulation could suggest an antibody-concentrating effect arising from FcRn interactions. From these results, it is reasonable to presume that the expression of human FcRn in

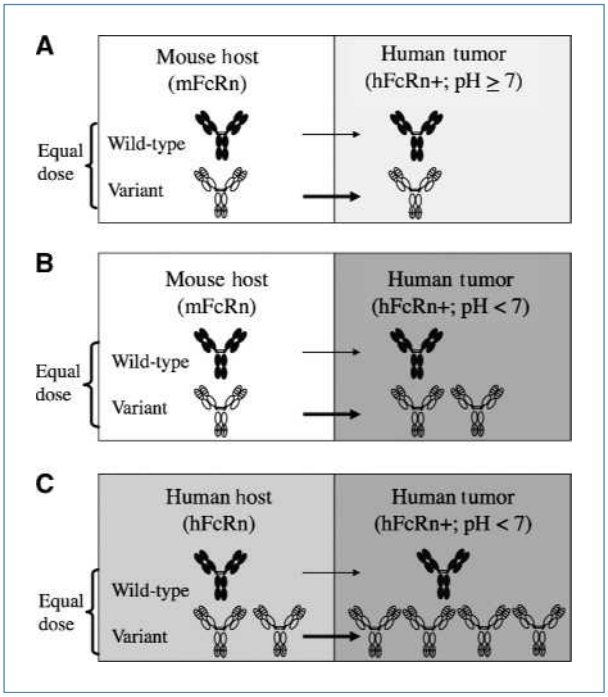

Figure 5. Model for distribution of WT anti-VEGF (filled "Y") and the T307Q/N434A FcRn-binding antibody variant (open "Y") in mouse xenografts (A and B) and in humans (C). The Calu-6 xenograft model is represented by A, where, at equal dosing, the two antibodies have similar systemic exposure, similar tumor concentrations, and similar potency. B, as suggested in Discussion, rapidly growing tumors such as HM-7 may have specific features (e.g., lower local pH, favoring pH-dependent binding to FcRn), increased tumor concentration of the T307Q/N434A variant, and increased potency. C, a similar effect may be predicted in certain human tumors, with the additional feature of increased systemic exposure resulting from slower clearance as observed in nonhuman primates.

the tumor cell lines (Fig. 4C) used in the mouse xenografts is solely responsible for the observed increase in the retention of variant antibody compared with WT. However, we found that all cell lines tested did express relatively high levels of FcRn (Fig. 4C). In addition, we did not find a direct correlation between the concentration effect and FcRn expression level, as HM-7 cells had the lowest level of FcRn expression among the three cell lines tested (Fig. 4C). Therefore, a simple, FcRn-mediated, local retention model is not sufficient to account for the observed increase in antibody retention/potency.

It is likely that a variety of factors, such as tumor pH, growth rate, FcRn expression pattern within the cells (basolateral versus apical), and other tumor constituents, play collaborative roles with FcRn in determining the distribution of IgGs. For example, the tumor microenvironment is more acidic, with pH ranging from 6.0 to 7.6 (median, 7.1) compared with normal tissues with pH ranging from 7.3 to 7.8 (median, 7.55; ref. 36). Furthermore, different types of tumors can have a wide range of pH due to heterogeneous vascular supply and blood perfusion (36, 37). Multiple *in vitro* studies indicate that the amount of cell-associated Fc/IgG increases when cells are incubated at acidic pH (38–40). Therefore, it is conceivable that pH differences among the tumor lines tested

may affect the accumulation level of antibody within each tumor. The extent of acidification in the tumor microenvironment may also be partly due to the tumor growth rate. The fastest growing tumors (e.g., HM-7) may yield a lower pH tumor microenvironment, which in turn favors the retention of FcRn variant antibodies. Additionally, the acidic tumor microenvironment also activates VEGF expression (36), which could mediate the retention of these anti-VEGF antibodies specifically.

In our model, the presence of both murine FcRn (in the host) and human FcRn (in the tumor) complicates extrapolation to humans. We argue that the human-host/human-tumor system favors an even greater distribution of FcRn variant to the tumor because at equal doses we have shown that the variant achieves higher systemic exposure in primates (as illustrated in Fig. 5). Because the potency effect in mouse xenografts is specific to a particular tumor type (colon cancer cell lines HM-7 and HT-55; but not lung cancer line Calu-6), this potency effect is not only an artifact of the human/mouse xenograft system. Instead, there must be tumor-specific factors, as discussed above, that result in tumor localization of the variant antibody and increased potency. In the human system, we expect to observe the increased systemic exposure, and the "extra" potency effect may be expected in cases where the tumor is similar to the HM-7 and HT-55 xenografts described here (Fig. 5).

An anti-VEGF FcRn-binding variant seems to offer the potential for less-frequent dosing than the WT antibody in patients and may have additional activity benefits. Less-frequent dosing, per se, has potential benefits of improved convenience for patients, as well as perhaps improved compliance with long-term dosing, which may ultimately improve the clinical outcome of treatment. However, the pharmacokinetics, safety, and efficacy of this molecule have yet to be studied in humans.

Our *in vivo* pharmacokinetic study in cynomolgus monkeys has important implications for long half-lived IgG variants in the clinical setting. The local concentration of such an antibody variant is expected to be higher than WT due to the increase in systemic serum level, yet our work suggests that the concentration may be further increased through tissue-specific FcRn effects when the tumor itself expresses FcRn. Further research is needed to decipher the factors affecting the recycling/retention properties of the variant within local tissues or tumors, as well as how these changes in local antibody concentrations affect the potency and therapeutic window of FcRn-binding IgG variants in humans.

Disclosure of Potential Conflicts of Interest

All authors: employment and ownership interest, Genentech, Inc. H.B. Lowman: consultant/advisory board, Genentech, Inc.

Acknowledgments

We thank Bob Mass and Greg Plowman for helpful discussion; the DNA synthesis and sequencing groups plus the Protein Chemistry group for material preparations; and Michelle Schweiger, Nicole Valle, Kirsten Messick, Noore Kadri, and Mike Reich for their assistance with the mouse pharmacokinetic studies.

The costs of publication of this article were defrayed in part by the payment of page charges. This article must therefore be hereby marked *advertisement* in accordance with 18 U.S.C. Section 1734 solely to indicate this fact.

Received 12/18/2009; revised 01/27/2010; accepted 02/16/2010; published OnlineFirst 03/30/2010.

References

1. Ferrara N, Hillan KJ, Gerber HP, Novotny W. Discovery and development of bevacizumab, an anti-VEGF antibody for treating cancer. Nat Rev Drug Discov 2004;3:391–400.
2. Martin WL, West AP, Jr., Gan L, Bjorkman PJ. Crystal structure at 2.8 A of an FcRn/heterodimeric Fc complex: mechanism of pH-dependent binding. Mol Cell 2001;7:867–77.
3. Roopenian DC, Akilesh S. FcRn: the neonatal Fc receptor comes of age. Nat Rev Immunol 2007;7:715–25.
4. West AP, Jr., Bjorkman PJ. Crystal structure and immunoglobulin G binding properties of the human major histocompatibility complex-related Fc receptor. Biochemistry 2000;39:9698–708.
5. Ober RJ, Martinez C, Lai X, Zhou J, Ward ES. Exocytosis of IgG as mediated by the receptor, FcRn: an analysis at the single-molecule level. Proc Natl Acad Sci U S A 2004;101:11076–81.
6. Ober RJ, Martinez C, Vaccaro C, Zhou J, Ward ES. Visualizing the site and dynamics of IgG salvage by the MHC class I-related receptor, FcRn. J Immunol 2004;172:2021–9.
7. Prabhat P, Gan Z, Chao J, et al. Elucidation of intracellular recycling pathways leading to exocytosis of the Fc receptor, FcRn, by using multifocal plane microscopy. Proc Natl Acad Sci U S A 2007;104:5889–94.
8. Ghetie V, Hubbard JG, Kim JK, Tsen MF, Lee Y, Ward ES. Abnormally short serum half-lives of IgG in β2-microglobulin-deficient mice. Eur J Immunol 1996;26:690–6.
9. Israel EJ, Wilsker DF, Hayes KC, Schoenfeld D, Simister NE. Increased clearance of IgG in mice that lack β2-microglobulin: possible protective role of FcRn. Immunology 1996;89:573–8.
10. Junghans RP, Anderson CL. The protection receptor for IgG catabolism is the β2-microglobulin-containing neonatal intestinal transport receptor. Proc Natl Acad Sci U S A 1996;93:5512–6.
11. Roopenian DC, Christianson GJ, Sproule TJ, et al. The MHC class I-like IgG receptor controls perinatal IgG transport, IgG homeostasis, and fate of IgG-Fc-coupled drugs. J Immunol 2003;170:3528–33.
12. Waldmann TA, Terry WD. Familial hypercatabolic hypoproteinemia. A disorder of endogenous catabolism of albumin and immunoglobulin. J Clin Invest 1990;86:2093–8.
13. Wani MA, Haynes LD, Kim J, et al. Familial hypercatabolic hypoproteinemia caused by deficiency of the neonatal Fc receptor, FcRn, due to a mutant β2-microglobulin gene. Proc Natl Acad Sci U S A 2006;103:5084–9.
14. Dall'Acqua WF, Woods RM, Ward ES, et al. Increasing the affinity of a human IgG1 for the neonatal Fc receptor: biological consequences. J Immunol 2002;169:5171–80.
15. Hinton PR, Johlfs MG, Xiong JM, et al. Engineered human IgG antibodies with longer serum half-lives in primates. J Biol Chem 2004;279:6213–6.
16. Dall'Acqua WF, Kiener PA, Wu H. Properties of human IgG1s engineered for enhanced binding to the neonatal Fc receptor (FcRn). J Biol Chem 2006;281:23514–24.
17. Hinton PR, Xiong JM, Johlfs MG, Tang MT, Keller S, Tsurushita N. An engineered human IgG1 antibody with longer serum half-life. J Immunol 2006;176:346–56.
18. Ghetie V, Popov S, Borvak J, et al. Increasing the serum persistence of an IgG fragment by random mutagenesis. Nat Biotechnol 1997;15:637–40.

19. Datta-Mannan A, Witcher DR, Tang Y, Watkins J, Jiang W, Wroblewski VJ. Humanized IgG1 variants with differential binding properties to the neonatal Fc receptor: relationship to pharmacokinetics in mice and primates. Drug Metab Dispos 2007;35:86–94.
20. Datta-Mannan A, Witcher DR, Tang Y, Watkins J, Wroblewski VJ. Monoclonal antibody clearance. Impact of modulating the interaction of IgG with the neonatal Fc receptor. J Biol Chem 2007;282: 1709–17.
21. Shields RL, Namenuk AK, Hong K, et al. High resolution mapping of the binding site on human IgG1 for FcγRI, FcγRII, FcγRIII, and FcRn and design of IgG1 variants with improved binding to the FcγR. J Biol Chem 2001;276:6591–604.
22. Yeung YA, Leabman MK, Marvin JS, et al. Engineering human IgG1 affinity to human neonatal Fc receptor: impact of affinity improvement on pharmacokinetics in primates. J Immunol 2009;182: 7663–71.
23. Presta LG, Chen H, O'Connor SJ, et al. Humanization of an anti-vascular endothelial growth factor monoclonal antibody for the therapy of solid tumors and other disorders. Cancer Res 1997;57: 4593–9.
24. Kunkel TA, Roberts JD, Zakour RA. Rapid and efficient site-specific mutagenesis without phenotypic selection. Methods Enzymol 1987; 154:367–82.
25. Rodriguez CR, Fei DT, Keyt B, Baly DL. A sensitive fluorometric enzyme-linked immunosorbent assay that measures vascular endothelial growth factor165 in human plasma. J Immunol Methods 1998;219:45–55.
26. Liang WC, Wu X, Peale FV, et al. Cross-species vascular endothelial growth factor (VEGF)-blocking antibodies completely inhibit the growth of human tumor xenografts and measure the contribution of stromal VEGF. J Biol Chem 2006;281:951–61.
27. Gerber HP, Wu X, Yu L, et al. Mice expressing a humanized form of VEGF-A may provide insights into the safety and efficacy of anti-VEGF antibodies. Proc Natl Acad Sci U S A 2007;104:3478–83.
28. Gerber HP, Kowalski J, Sherman D, Eberhard DA, Ferrara N. Complete inhibition of rhabdomyosarcoma xenograft growth and neovascularization requires blockade of both tumor and host vascular endothelial growth factor. Cancer Res 2000;60:6253–8.
29. Lin YS, Nguyen C, Mendoza JL, et al. Preclinical pharmacokinetics, interspecies scaling, and tissue distribution of a humanized monoclonal antibody against vascular endothelial growth factor. J Pharmacol Exp Ther 1999;288:371–8.
30. Goebl NA, Babbey CM, Datta-Mannan A, Witcher DR, Wroblewski VJ, Dunn KW. Neonatal Fc receptor mediates internalization of Fc in transfected human endothelial cells. Mol Biol Cell 2008;19: 5490–505.
31. Vaccaro C, Zhou J, Ober RJ, Ward ES. Engineering the Fc region of immunoglobulin G to modulate *in vivo* antibody levels. Nat Biotechnol 2005;23:1283–8.
32. Gurbaxani B, Dela Cruz LL, Chintalacharuvu K, Morrison SL. Analysis of a family of antibodies with different half-lives in mice fails to find a correlation between affinity for FcRn and serum half-life. Mol Immunol 2006;43:1462–73.
33. Pan H, Chen K, Chu L, Kinderman F, Apostol I, Huang G. Methionine oxidation in human IgG2 Fc decreases binding affinities to protein A and FcRn. Protein Sci 2009;18:424–33.
34. Vaccaro C, Bawdon R, Wanjie S, Ober RJ, Ward ES. Divergent activities of an engineered antibody in murine and human systems have implications for therapeutic antibodies. Proc Natl Acad Sci U S A 2006;103:18709–14.
35. Kamei DT, Lao BJ, Ricci MS, et al. Quantitative methods for developing Fc mutants with extended half-lives. Biotechnol Bioeng 2005; 92:748–60.
36. Song CW, Griffin R, Park HJ. Influence of tumor pH on therapeutic response. In: Teicher BA, editor. Cancer Drug Resistance. New Jersey: Humana Press; 2006. pp. 21–42.
37. Gillies RJ, Raghunand N, Karczmar GS, Bhujwalla ZM. MRI of the tumor microenvironment. J Magn Reson Imaging 2002;16:430–50.
38. Praetor A, Ellinger I, Hunziker W. Intracellular traffic of the MHC class I-like IgG Fc receptor, FcRn, expressed in epithelial MDCK cells. J Cell Sci 1999;112:2291–9.
39. McCarthy KM, Yoong Y, Simister NE. Bidirectional transcytosis of IgG by the rat neonatal Fc receptor expressed in a rat kidney cell line: a system to study protein transport across epithelia. J Cell Sci 2000; 113:1277–85.
40. Tesar DB, Tiangco NE, Bjorkman PJ. Ligand valency affects transcytosis, recycling and intracellular trafficking mediated by the neonatal Fc receptor. Traffic 2006;7:1127–42.